THE JOURNAL OF PHYSICAL CHEMISTRY C

Article

Cite This: J. Phys. Chem. C 2018, 122, 3985−3993

pubs.acs.org/JPCC

The Role of a Phonon Bottleneck in Relaxation Processes for Ln-Doped $NaYF_4$ Nanocrystals

Jacobine J. H. A. van Hest,[†,‡] Gerhard A. Blab,[‡] Hans C. Gerritsen,[‡] Celso de Mello Donega,[†] and Andries Meijerink*[,†]

[†]Condensed Matter and Interfaces, Debye Institute for Nanomaterials Science, and [‡]Molecular Biophysics, Utrecht University, Princetonplein 5, 3584 CC Utrecht, The Netherlands

ABSTRACT: The localized inner 4f shell transitions of lanthanide ions are largely independent of the local surroundings. The luminescence properties of Ln^{3+} ions doped into nanocrystals (NCs) are therefore similar to those in bulk crystals. Quantum size effects, responsible for the unique size-dependent luminescence of semiconductor NCs, are generally assumed not to influence the optical properties of Ln^{3+}-doped insulator NCs. However, phonon confinement effects have been reported to hamper relaxation between closely spaced Stark levels in Ln^{3+}-doped NCs. At cryogenic temperatures emission and excitation from higher Stark levels was observed for Ln^{3+} ions in NCs only and were explained by a cutoff in the acoustic phonon spectrum. Relaxation would be inhibited as no resonant low energy (long wavelength) acoustic phonon modes can exist in nanometer sized crystals, and this prevents relaxation by direct phonon emission between closely spaced Stark levels. This phenomenon is known as a phonon bottleneck. Here, we investigate the role of phonon confinement in Ln-doped NCs. High resolution emission spectra at temperatures down to 2.2 K are reported for various Ln^{3+} ions (Er^{3+}, Yb^{3+}, Eu^{3+}) doped into monodisperse 10 nm $NaYF_4$ NCs and compared with spectra for bulk (microcrystalline) material. Contrary to previous reports, we find no evidence for phonon bottleneck effects in the emission spectra. Emission from closely spaced higher Stark levels is observed only at high excitation powers and is explained by laser heating. The present results indicate that previously reported effects in NCs may not be caused by phonon confinement.

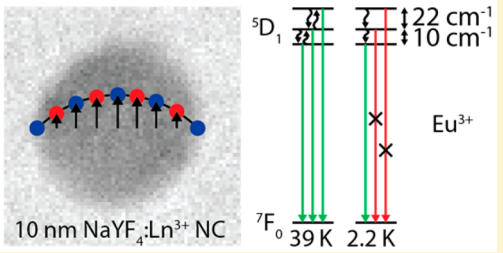

INTRODUCTION

Lanthanide (Ln)doped nanocrystals (NCs) have been investigated for various applications in the past decades.[1−3] It is commonly assumed that the size of the inorganic host NC does not affect the optical properties, since the transitions of Ln^{3+} ions are localized within the 4f inner orbitals which are shielded by the 5s and 5p orbitals. However, spatial confinement effects can be introduced by phonons when reducing the size to the nanoscale, since phonons are delocalized. In the phonon spectrum for nanoparticles, there is a cutoff for low energy acoustic phonon modes which shifts to higher energies for smaller NCs and for energies just above the cutoff energy discrete acoustic phonon modes arise.[4−7] The absence of resonant acoustic phonon modes can inhibit direct one-phonon relaxation processes between closely spaced energy levels. This phenomenon is known as the phonon bottleneck.[8,9] Next to Ln-doped NCs, the presence of a phonon bottleneck has also been reported for discrete electronic states in quantum dots.[8,10−12] Phonon bottleneck effects are only expected to be observed at low temperatures where relaxation to lower energy levels occurs by emission of one resonant phonon (known as the direct process). At higher temperatures, when higher energy phonon modes are thermally populated, two-phonon processes take over and absorption and emission of two phonons of slightly different energy can make up the small energy difference between closely spaced energy levels. Two-phonon relaxation processes are much more efficient than direct relaxation but do require thermal energy, since higher energy phonon modes must be occupied. Note that the phonon bottleneck explained above is different from phonon bottleneck effects extensively reported in the literature in e.g. ruby.[13] For this type of phonon bottleneck, excitation in a higher electronic energy level causes a nonequilibrium population of phonon modes resonant with the energy difference between electronic states. This gives rise to stronger emission from the higher energy level than expected based on a Boltzmann distribution. This observation is similar as for the phonon bottleneck that is the topic of the present work, but the reason is not the absence of resonant phonon modes but a high nonequilibrium occupation of resonant phonon modes.

In this report, we focus on the role of the phonon bottleneck in Ln-doped NCs generated by the cutoff of low energy acoustic phonon modes and the presence of discrete phonon modes in the acoustic phonon spectrum on direct relaxation rates to the lowest Stark level. For Ln-doped NCs, cutoff energies in the acoustic phonon spectrum have been reported to be 8 cm^{-1} for 11.6 nm Eu_2O_3 NCs,[7] 25 cm^{-1} for 10 nm $Y_2O_2S:Er^{3+}$ NCs,[14] and 30 cm^{-1} for 2.5 nm $NaGdF_4$ NCs,[15]

Received: November 11, 2017
Revised: January 25, 2018
Published: February 5, 2018

DOI: 10.1021/acs.jpcc.7b11171
J. Phys. Chem. C 2018, 122, 3985−3993

and discrete phonon modes up to 200 cm^{-1} for 10 nm $Y_2O_2S:Er^{3+}$ NCs[14] have been reported. Clearly, the cutoff energies for ~10 nm NCs are comparable with the energy separation between Stark levels of Ln-doped NCs.[16,17] Based on the cutoff energy and the fact that above the cutoff the phonon spectrum is not a continuum but consists of discrete energies, one can expect reduced nonradiative relaxation rates between Stark levels because of the absence of phonon modes resonant with the energy difference between Stark levels. As a result, extra emission and excitation lines from upper Stark levels should be observed at cryogenic temperatures in the spectra of NCs where relaxation between Stark levels is dominated by the direct process.

Ln-doped NCs have been reported to have different luminescence spectra than bulk material due to the presence of the phonon bottleneck. Tissue et al. have reported the presence of a phonon bottleneck in Ln-doped NCs.[18] They observed the phonon bottleneck in the excitation spectrum of Ln-doped NCs recorded at 12 K and have suggested a storage of population in the $^7F_1$ level and in low-lying excited states of clustered 4 nm $Y_2O_3:Eu^{3+}$ (0.1%) and Eu_2O_3 NCs synthesized using the CO_2-laser-heated gas phase condensation method. The most extensive research on the phonon bottleneck in Ln-doped NCs has been performed by Liu et al.[14,19] In their work, the presence of the phonon bottleneck for energy gaps up to 200 cm^{-1} in the excitation spectrum of clustered 10−20 nm $Y_2O_2S:Er^{3+}$ (2%) NCs synthesized using a flame spray pyrolysis technique has been observed at 2.6 K. In addition, the increase in green to red emission ratio in $NaYF_4:Yb^{3+}$(20%),Er^{3+}(2%) NCs by reducing the size from 47.1 to 5.6 nm has been explained by a phonon bottleneck of optical phonons.[20] However, this observation has been questioned in a later study.[21] The presence of emission lines from upper Stark levels up to 225 cm^{-1} above the lowest Stark level at 80 K in 5 nm $Y_2SiO_5:Pr^{3+}$ (0.01%) NCs synthesized by the sol−gel method has been explained by the absence of low-energy phonons and a low phonon density of states.[22] Moreover, hot bands with energies up to 217 cm^{-1} have been observed in the excitation spectra of 10−30 nm by 70−80 nm $Gd_2O_3:Eu^{3+}$ (4%) nanotubes synthesized by a hydrothermal method and have been ascribed to phonon bottleneck effects.[23]

In the studies mentioned above, the phonon bottleneck has been claimed to be present for energy gaps as high as ~200 cm^{-1}. However, these high energy acoustic phonon modes are not cut off in 10−20 nm nanoparticles. Only low energy acoustic phonon modes are cut off. For this reason, phonon bottleneck effects are only expected for energy gaps up to 50 cm^{-1}. Moreover, pulsed laser excitation sources have been used in most studies, which may induce temporary heating of the sample resulting in emission and excitation lines from thermally populated upper Stark levels in Ln-doped NCs. In addition, polydisperse NCs or samples with poorly defined sizes have been used in some studies. This complicates the analysis of the results as confinement effects will strongly vary between crystallites of different sizes. Finally, not all measurements have been performed below ~7 K, which is required to avoid thermal population of closely separated upper Stark levels. As a result, the presence of the phonon bottleneck in Ln-doped NCs remains uncertain, and a careful study on a well-defined model system is required to provide evidence for the role of phonon confinement in the optical spectra of Ln^{3+} ions in NCs.

In this work, the origin of emission from upper Stark levels in Ln-doped NCs at cryogenic temperatures is investigated. To this end, high resolution emission spectra of monodisperse 10 nm $NaYF_4$ NCs and microcrystalline $NaYF_4$ powders doped with different Ln^{3+} ions (Er^{3+}, Yb^{3+}, Eu^{3+}) are recorded at cryogenic temperatures (down to 2.2 K) with pulsed and continuous wave excitation sources and at various excitation power densities. Emission from 10 to 50 cm^{-1} higher Stark levels is observed for Er^{3+} and Eu^{3+} at cryogenic temperatures. However, a decrease in relative emission intensity from upper Stark levels is observed when the excitation power is reduced, and no emission from higher Stark levels is observed for the lowest excitation powers. This indicates that heating of the NC samples by the excitation source is responsible for emission from higher Stark levels, not a phonon bottleneck. Based on our experiments, we conclude that phonon bottleneck effects do not affect emission spectra on Ln^{3+} ions in 10 nm Ln-doped $NaYF_4$ NCs and that these Ln-doped NCs excited with low excitation powers have the same emission spectra as their microcrystalline analogues. Further research into a role of phonon confinement in Ln-doped NCs remains interesting. Even if the phonon relaxation is not slowed down enough to allow the observation of emission from higher Stark levels, phonon-induced dephasing processes (as measured in photon echo or homogeneous line broadening experiments) may be affected by phonon confinement.[24,25] The present study shows that in order to establish the role of phonon confinement in Ln-doped nanocrystals, careful measurements on model systems are required and that care has to be taken to rule out an influence of laser-induced heating.

EXPERIMENTAL SECTION

Chemicals. The chemicals used in the various synthesis procedures were NaF (Fluka Analytical, ≥98%), NaOH (Sigma-Aldrich, ≥97%), sodium oleate (TCI, ≥97%), YF_3 (ChemPur, 99.9%), $YCl_3·6H_2O$ (Aldrich, 99.99%), yttrium acetate hexahydrate (Aldrich, 99.9%), ErF_3 (Highways International, 99.9%), $ErCl_3·6H_2O$ (Strem, 99.9%), erbium acetate hexahydrate (Aldrich, 99.9%), EuF_3 (Highways International, 99.99%), $EuCl_3·6H_2O$ (Aldrich, 99.9%), $YbCl_3·6H_2O$ (Strem, 99.99%), NH_4F (Sigma-Aldrich, ≥98.0%), oleic acid (Aldrich, 90%) 1-octadecene (Aldrich, 90%), ethanol (Alfa Aesar, 96%), methanol (Sigma-Aldrich, 99.8%), hexane (Sigma-Aldrich, 95%) and cyclohexane (Sigma-Aldrich, 99.5%). All chemicals were used as received.

Synthesis of Microcrystalline β-$NaYF_4:Ln^{3+}$. Microcrystalline $NaYF_4$ doped with either 0.5% Er^{3+} or 0.3% Eu^{3+} was synthesized by a dry mixture method described by Aarts et al.[26] Stoichiometric amounts of sodium fluoride and lanthanide fluorides (99.5% or 99.7% YF_3 and 0.5% ErF_3 or 0.3% EuF_3) were mixed and ground in an agate mortar. Subsequently, the mixture was fired in an oven together with an excess of NH_4F under a nitrogen flow. The samples were first heated to 300 °C for 2 h and then to 550 °C for 3 h. After cooling down to room temperature, the samples were crushed in an agate mortar. X-ray diffraction (XRD) measurements were performed to check for phase purity. A second firing at 550 °C for 6 h under nitrogen was performed in case XRD measurements showed the presence of residual reactants. After a second firing, phase pure $NaYF_4$ was obtained in all cases.

Synthesis of Nanocrystalline β-$NaYF_4:Ln^{3+}$. For the synthesis of nanocrystalline $NaYF_4$, rare earth oleates were prepared first according to the method described by Park et al.[27] In a typical reaction, 6 mmol of rare-earth chlorides (4.80 mmol yttrium chloride, 1.08 mmol ytterbium chloride, and 0.12

DOI: 10.1021/acs.jpcc.7b11171
J. Phys. Chem. C 2018, 122, 3985−3993

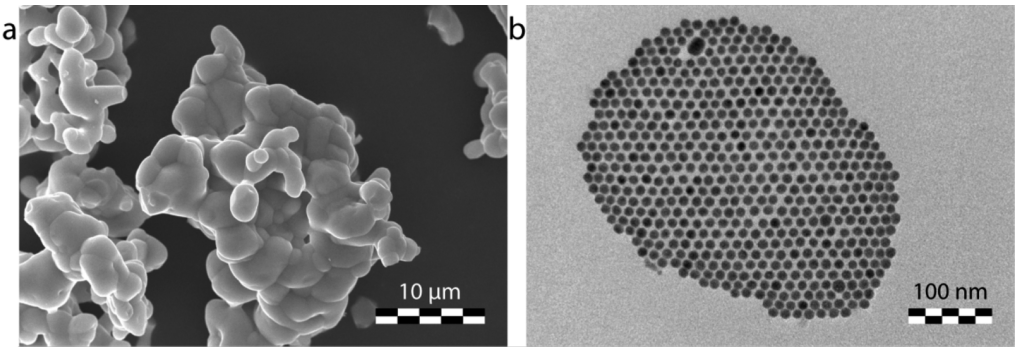

Figure 1. (a) SEM image of microcrystalline $NaYF_4:Er^{3+}$ (0.5%) and (b) TEM image of $NaYF_4:Er^{3+}$ (0.5%) NCs.

mmol erbium chloride or 5.97 mmol yttrium chloride and 0.03 mmol europium chloride) and 18 mmol sodium oleate were dissolved in a solvent mixture composed of 12 mL ethanol, 9 mL distilled water, and 21 mL hexane. The resulting solution was stirred at room temperature for 2 h. After the reaction was completed, the organic layer containing the rare-earth oleates was washed three times with distilled water. The viscous substance was dried, and a waxy slightly yellow solid was obtained.

The β-$NaYF_4:Yb^{3+}(18\%),Er^{3+}(2\%)$ and $NaYF_4:Eu^{3+}$ (0.5%) NCs were synthesized using a modification of the method described by Rinkel et al.[28] First, 2 mmol sodium oleate and 1 mmol rare-earth oleate were dissolved in a mixture of 20 mL oleic acid and 20 mL 1-octadecene and degassed at 100 °C for 1 h in a Schlenk line. Next, the system was purged with nitrogen, and the temperature was allowed to drop. At temperatures below 40 °C, 5 mmol NH_4F was added, and the system was degassed and then refilled with nitrogen three times. The mixture was heated to 300 °C and kept at this temperature for 100 min. After cooling to room temperature, the NCs were precipitated from the reaction mixture by adding ethanol, centrifuging, and removing the supernatant. The white sediment was redispersed in ∼10 mL of cyclohexane. The washing step was repeated twice. In the last purification step, 10 mL oleic acid was added to the NCs in cyclohexane to enhance the ligand density at the NC surface. Next, the mixture was sonicated for 15 min. The NCs were isolated from the mixture by adding ethanol, centrifuging, and removing the supernatant. The white sediment was redispersed in 10 mL cyclohexane.

The β-$NaYF_4:Er^{3+}$ (0.5%) NCs were synthesized using a method described by Li et al.[29] and Wang et al.[30] First, 4 mmol rare-earth acetates (3.98 mmol yttrium acetate and 0.02 mmol erbium acetate) was dissolved in a mixture of 24 mL oleic acid and 68 mL 1-octadecene and degassed at 110 °C for 90 min in a Schlenk line. Subsequently, the system was purged with nitrogen, degassed three times, and then refilled with nitrogen before the temperature was allowed to drop. At temperatures below 30 °C, 10 mmol NaOH in 10 mL methanol was added, followed by 16 mmol NH_4F in 28 mL methanol. The reaction mixture was stirred for 16 h to allow the formation of α-$NaYF_4$. Next, the excess methanol was removed by heating the reaction mixture to 100 °C under vacuum for 30 min. The system was degassed three times and refilled with nitrogen before heating to 300 °C for 110 min to allow for the growth of β-$NaYF_4$ NCs. After cooling, the NCs were isolated from the reaction mixture using the same method as for the β-$NaYF_4:Yb^{3+}(18\%),Er^{3+}(2\%)$ and $NaYF_4:Eu^{3+}$ (0.5%) NCs.

Characterization and Optical Spectroscopy. The purified NC samples were characterized with transmission electron microscopy (TEM). Samples for analysis were obtained by diluting the as-synthesized NCs in dispersion 100 times with cyclohexane and dropcasting the NC solutions on coated copper TEM grids. The TEM images were obtained with a Tecnai 10 microscope equipped with a tungsten filament operating at 100 kV. Images were recorded with a SIS CCD camera Megaview II using iTEM software.

The bulk microcrystalline samples were characterized with scanning electron microscopy (SEM). The samples for analysis were obtained by placing a thin layer of sample on a SEM stub with carbon tape. A 4 nm layer of platina was sputtered on top of the samples. SEM images were obtained with a XL30S FEG microscope operating at 20 kV. Images were recorded using Scandium software.

X-ray diffraction patterns of powder samples were recorded with a PW1729 Philips diffractometer equipped with a Cu Kα X-ray source (λ = 1.5418 Å). Reference diffractograms were taken from the International Center of Diffraction Data (ICDD).

High resolution emission spectra of powders were recorded using an Ekspla NT342B tunable laser exciting in the $^4I_{15/2}-^4F_{7/2}$ transition at 483.0 nm for the $NaYF_4:Er^{3+}$ samples and exciting in the $^7F_0-^5D_2$ transition at 465.2 nm for the $NaYF_4:Eu^{3+}$ samples (repetition rate 10 Hz, pulse width 6 ns). Typically, the laser was operated at pulse powers corresponding to ∼1 mJ per pulse. The $NaYF_4:Yb^{3+},Er^{3+}$ NCs were excited in the $^2F_{7/2}-^2F_{5/2}$ transition of Yb^{3+} at 980 nm with a MDL-III-980-500 mW continuous wave diode laser. The excitation power was varied by placing reflective neutral density filters (Newport, New Focus, 5212 dual filter wheel) in the laser beam. The emitted light was dispersed with a Triax 550 single emission monochromator (Jobin Yvon, 1200 line grating blazed at 400 nm) and detected with a Hamamatsu R928 detector and a Stanford Research SR400 gated photon counter set with a gate of 50 ms. Timing was controlled with a Stanford Research DG535 pulse generator. The spectral bandwidth of the monochromator was 0.075 nm (2−3 cm^{-1}). The samples were cooled to temperatures between 2.2 and 50 K with an Oxford Instruments liquid helium flow cryostat. The samples were immersed in liquid helium for temperatures below 4.2 K. In all experiments, the sample chamber is filled with helium gas or liquid which ensures a good heat transfer from the sample.

RESULTS AND DISCUSSION

Characterization. $NaYF_4:Ln^{3+}$ (Ln = Er(0.5%), Eu(0.5%), or Yb(18%)−Er(2%)) bulk and nanocrystals (NCs) were

DOI: 10.1021/acs.jpcc.7b11171
J. Phys. Chem. C 2018, 122, 3985−3993

synthesized by methods previously described in the literature.[26,28−30] The size, shape and monodispersity of the various samples are important, since they determine the cutoff energy of acoustic phonon modes and the discrete acoustic phonon modes in the phonon spectrum. The size, shape, and uniformity of the different samples were studied with electron microscopy. Figure 1 shows a scanning electron microscope (SEM) image of bulk $NaYF_4$ and a transmission electron microscope (TEM) image of $NaYF_4$ NCs, which are representative for the shape and uniformity of all bulk and NC samples. The bulk sample consists of micrometer sized crystallites as can be seen in Figure 1a. The TEM image of the NCs is shown in Figure 1b. The NCs are almost spherical and have sizes of 11.6 ± 1.4 nm for erbium-doped NCs, 11.8 ± 1.3 nm for the europium-doped NCs, and 9.6 ± 0.8 nm for the ytterbium and erbiumcodoped NCs. The $NaYF_4$:Yb^{3+},Er^{3+} NCs are slightly smaller than the $NaYF_4$:Er^{3+} and $NaYF_4$:Eu^{3+} NCs. A possible explanation for the smaller size of the ytterbium−erbium-codoped sample is the total dopant concentration. It has been reported that replacing the yttrium ion with other rare-earth ions can result in different sizes and shapes of the $NaYF_4$ end products.[31] In the ytterbium−erbium sample, 20% of the yttrium ions is replaced by dopant ions, while in the erbium and europium sample only 0.5% yttrium ions is replaced, resulting in a smaller size for the Yb-codoped sample.

The crystal structure of both bulk and NCs is an important parameter for understanding the luminescence properties. β-$NaYF_4$ crystallizes in the hexagonal structure under ambient conditions. X-ray diffractograms (XRDs) were recorded to study the structure and phase purity of the bulk and NC samples. XRDs of microcrystalline (blue) and nanocrystalline (red) samples are shown in Figure 2. A reference diffractogram

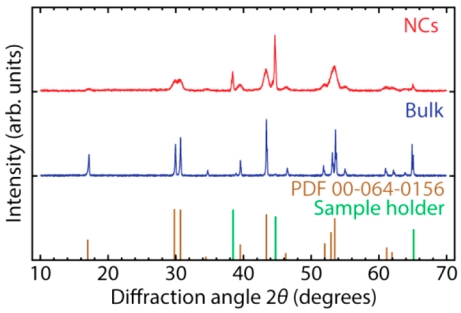

Figure 2. XRD patterns of $NaYF_4$ nanocrystals (red) and microcrystalline bulk material (blue). Below reference patterns of the hexagonal β-$NaYF_4$ structure (PDF 00-064-0156) and the sample holder are plotted in brown and green, respectively.

of β-$NaYF_4$ and a reference diffractogram of the sample holder are included in the same figure. The bulk and NC materials show diffraction peaks that are consistent with the hexagonal structure for β-$NaYF_4$. The XRDs of most bulk and NC samples do not show a secondary phase. However, for the $NaYF_4$:Er^{3+} NC sample, a small fraction of secondary NaF phase is present. Small traces of NaF in the $NaYF_4$:Er^{3+} NC sample do not interfere with the luminescence measurements, since Ln^{3+} ions do not easily incorporate in this crystal structure where the trivalent Ln ion would replace a monovalent Na ion. The width of the diffraction peaks is very different for microcrystalline and NC samples. The diffraction peaks for the microcrystalline bulk samples are sharp, consistent with the presence of large micrometer sized crystals. In contrast, the observation of broad diffraction peaks for the NC samples confirms the formation of nanometer sized particles.

Optical Spectroscopy of $NaYF_4$:Er^{3+}. High resolution emission spectra of micro- and nanocrystalline samples were recorded at low temperatures to investigate the role of the phonon bottleneck in relaxation processes for Ln-doped NCs. The measurement conditions, e.g., temperature, excitation power, and spectral resolution of monochromator, are important. The temperature is essential in the experiments as it determines the phonon occupation of the phonon modes and thermal population of higher Stark levels. The contribution of various relaxation processes, i.e., the one-phonon direct process and the two-phonon processes (e.g., Orbach and Raman), varies in different temperature regimes. The contribution of the direct process dominates at low temperatures.[32] It is this direct relaxation process between Stark levels that can be inhibited for Ln-doped NCs when there are no resonant low energy acoustic phonon modes that can take up the small energy difference between two Stark levels. At higher temperatures, two-phonon processes dominate, resulting in "normal" and fast relaxation behavior yielding in a Boltzmann thermal distribution over the different Stark levels. Consequently, the phonon bottleneck between closely separated Stark levels in Ln-doped NCs can only be observed at low temperatures, e.g., 4.2 K or even below for 10 nm NCs. In addition, thermal line broadening is reduced at low temperatures. As a result, the emission lines originating from different Stark levels, which are typically separated by 10 to 100 cm^{-1}, can be better distinguished at low temperatures. In order to detect the distinct emission lines, a high spectral resolution in the emission spectra is needed. In the present experiments a bandpass of 0.075 nm (2−3 cm^{-1}) is used as the inhomogeneous spectral width of the emission lines is typically larger than 2−3 cm^{-1}. Finally, the power of the excitation source should be sufficient low to prevent laser-induced heating. In order to investigate the influence of the excitation intensity on the luminescence properties of the NCs, emission spectra are recorded with various excitation sources and excitation powers.

Figure 3a shows emission spectra of $NaYF_4$:Er^{3+}(0.5%) bulk recorded in the temperature range between 4.2 and 50 K by exciting into the $^4F_{7/2}$ level of Er^{3+} at 483.0 nm (20 704 cm^{-1}) with a pulsed laser with peak intensity of 2.0 MW/cm^2. The emission spectrum recorded at 4.2 K shows sharp emission lines at 18 523, 18 458, 18 428, and 18 390 cm^{-1}, which are assigned to the $^4S_{3/2}$−$^4I_{15/2}$ transition. In the bulk sample, only the lowest Stark level of the excited state is populated at 4.2 K according to the Boltzmann distribution. For this reason, the various emission lines correspond to transitions from the lowest Stark level of the excited state ($^4S_{3/2}$) to the four lowest Stark levels of the ground state ($^4I_{15/2}$). Note that for the remainder of this report the various Stark levels of the $^{2S+1}L_J$ states are labeled as $^{2S+1}L_J(x)$, where x labels the Stark levels from low to high energy. For example, the Stark level of the $^4I_{15/2}$ state with lowest energy is labeled as $^4I_{15/2}(1)$.

The emission spectra of $NaYF_4$:Er^{3+}(0.5%) bulk recorded at 22 and 50 K show the same emission peaks observed at 4.2 K plus several additional peaks located at 18 577, 18 557, 18 512, 18 495, and 18 484 cm^{-1}, as is shown in Figure 3a. At elevated temperatures, the upper Stark levels of the $^4S_{3/2}$ state are thermally populated, and the additional peaks correspond to transitions from these levels to $^4I_{15/2}(x)$ levels. The spectral positions observed for the Er^{3+} emission lines at 22 and 50 K

DOI: 10.1021/acs.jpcc.7b11171
J. Phys. Chem. C 2018, 122, 3985−3993

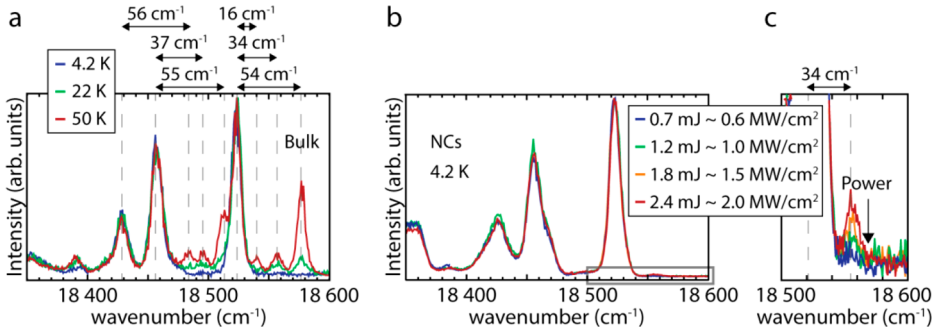

Figure 3. Emission spectra (λ_{exc} = 483.0 nm, pulsed laser) of $NaYF_4:Er^{3+}$ (0.5%) showing part of the $^4S_{3/2}-^4I_{15/2}$ emission spectrum. (a) Emission spectra for microcrystalline material recorded at various temperatures with peak intensity of 2.0 MW/cm^2. (b) Emission spectra for nanocrystals recorded at 4.2 K excited with excitation powers ranging from 0.7 to 2.4 mJ per pulse, corresponding to peak intensities ranging from 0.6 to 2.0 MW/cm^2. (c) Zoom of the area indicated in (b) showing a drop in relative emission intensity from upper Stark levels with decreasing excitation power. The emission intensity of the upper Stark level is approximately 65 times lower than the emission intensity of the main peak for the spectrum recorded with highest excitation intensity.

are in good agreement with previous results on the Er^{3+} emission in $NaYF_4:Er^{3+}$.[33]

The $^4S_{3/2}$ state splits in a maximum of two doubly degenerate Stark levels, indicating that a maximum of two transitions from the $^4S_{3/2}$ state to a $^4I_{15/2}(x)$ level can be present at higher temperatures. However, at least three transitions from the $^4S_{3/2}$ state to a $^4I_{15/2}(x)$ level are observed at 22 K. For example, the emission peaks at 18 523, 18 557, and 18 577 cm^{-1} are all assigned to transitions of the $^4S_{3/2}$ state to the $^4I_{15/2}(1)$ level. This suggests the presence of multiple sites in the material. This is consistent with previous reports on Ln-doped $NaYF_4$.[33,34] In the emission spectrum of bulk $NaYF_4:Er^{3+}$ recorded at 50 K additional emission lines at 18 557 and 18 577 cm^{-1} are observed and assigned to transitions from higher $^4S_{3/2}$ levels to the $^4I_{15/2}(1)$ level. As a result, the energy gaps between the $^4S_{3/2}(1)$ energy level (18 523 cm^{-1}) and these higher $^4S_{3/2}$ energy levels are 34 and 54 cm^{-1}, respectively. These energy gaps are similar to the energy separations between emission lines involving transitions from $^4S_{3/2}(x)$ levels to other Stark levels of $^4I_{15/2}$ state, as is indicated in Figure 3a. The spectrum recorded at 50 K shows a small extra emission peak at 18 539 cm^{-1}. The energy of this transition is 16 cm^{-1} higher than the $^4S_{3/2}(1)-^4I_{15/2}(1)$ transition. The transition is not present in the spectrum recorded at 22 K, which indicates that this emission line does not correspond to emission from a $^4S_{3/2}$ Stark level 16 cm^{-1} above the $^4S_{3/2}(1)$ level. Possibly the line corresponds to emission from a $^4S_{3/2}(2)$ level to a $^4I_{15/2}(2)$ Stark level for one of the sites.

To investigate the role of phonon bottleneck effects in $NaYF_4:Er^{3+}(0.5\%)$ NCs, emission spectra of the nanocrystalline sample were recorded at 4.2 K. Figure 3b shows normalized emission spectra of NCs excited at 483.0 nm (20 704 cm^{-1}) with excitation powers varying from 0.7 to 2.4 mJ per pulse, corresponding to peak intensities of 0.6–2.0 MW/cm^2. Several sharp emission lines are observed, which are assigned to the $^4S_{3/2}-^4I_{15/2}$ transition. The emission spectra of the NCs recorded at 4.2 K are similar to the emission spectrum of the bulk sample recorded at 4.2 K. Note that the widths of the emission lines are broader for NCs than for bulk. For example, the emission line at 18 523 cm^{-1} has a full width at half-maximum (fwhm) of 8 cm^{-1} for the bulk sample, while the NC sample has a fwhm of 10 cm^{-1}. The broader emission linewidths for NCs is explained by disorder in the NC surface, resulting in small differences in the local coordination of Er^{3+} ions which causes variations in crystal fields and thus in the exact positions of the energy levels for Er^{3+} ions in the NCs.[35] The similarity between emission spectra for bulk and NC samples at 4.2 K indicates that only transitions from the $^4S_{3/2}(1)$ level to $^4I_{15/2}(x)$ levels are present for the NC sample. No clear emission lines from upper Stark levels of the $^4S_{3/2}$ state are observed.

Upon close inspection, a weak feature can be observed on the high energy side of the $^4S_{3/2}(1)-^4I_{15/2}(1)$ emission line at 18 523 cm^{-1}. Figure 3c shows a zoom-in of this area that is indicated by the box in Figure 3b. A weak peak is observed at 18 557 cm^{-1}, at the same position as a peak for bulk $NaYF_4:Er^{3+}$ (0.5%), and is assigned to the $^4S_{3/2}(2)-^4I_{15/2}(1)$ transition. The observation of this peak could indicate reduced phonon relaxation as at 4.2 K the thermal (Boltzmann) population of a Stark level 34 cm^{-1} above the lowest level is less than 10^{-5}. Clearly the observed relative intensity, approximately 65 lower than the main peak, is higher than expected based on Boltzmann statistics. To investigate if the presence is caused by laser-induced heating, the laser power was reduced. The relative intensity of the higher energy emission peak drops when the laser power is reduced from 2.4 to 0.7 mJ per pulse, corresponding to a decrease in peak intensity from 2.0 to 0.6 MW/cm^2. The drop in relative intensity of emission lines originating from upper Stark levels of the $^4S_{3/2}$ state indicates that the NCs are heated by the laser. Laser heating can be expected, especially for NCs where thermal conductivity from the NCs to the copper block involves many interparticle barriers. For the bulk sample, no emission from upper Stark levels is observed under similar measurement conditions, even at peak intensities of 2.0 MW/cm^2. A better thermal conductivity (faster heat transfer through larger crystallites with less interparticle barriers) can explain the difference. These results indicate that no phonon bottleneck is present and that in the 10 nm $NaYF_4:Er^{3+}$ NCs relaxation to the lowest $^4S_{3/2}$ Stark level is fast, even at 4.2 K. The pulsed excitation source can temporarily heat the sample, due to the high power during the laser pulse. For this reason, the influence of the nature of the excitation source on the optical properties of the NCs is investigated by replacing the excitation source with a continuous wave (CW) excitation source. Emission spectra of $NaYF_4:Yb^{3+}(18\%),Er^{3+}(2\%)$ NCs were measured at 4.2 K by exciting into the $^2F_{5/2}$ level of Yb^{3+} with a 980 nm CW laser and recording the $^4S_{3/2}-^4I_{15/2}$ transition of Er^{3+}. The upconversion

DOI: 10.1021/acs.jpcc.7b11171
J. Phys. Chem. C 2018, 122, 3985−3993

mechanism has been studied before and will not be discussed here.[36] Figure 4 shows the emission spectra of the NCs excited

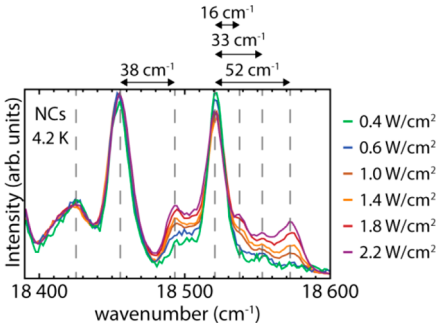

Figure 4. Emission spectra (λ_{exc} = 980 nm with continuous wave laser) of nanocrystalline $NaYF_4$:Yb^{3+},Er^{3+} showing the $^4S_{3/2}$–$^4I_{15/2}$ transition of Er^{3+} recorded at with mean intensities varying from 0.4 to 2.2 W/cm^2.

with mean intensities varying from 0.4 to 2.2 W/cm^2. The emission spectra show multiple sharp emission lines originating from the $^4S_{3/2}$–$^4I_{15/2}$ transition of Er^{3+} and look similar to the emission spectra of bulk $NaYF_4$:Er^{3+} recorded at 22 and 50 K. Emission lines positioned at 18 522, 18 455, and 18 425 cm^{-1} are ascribed to transitions from the $^4S_{3/2}(1)$ level to $^4I_{15/2}(x)$ levels. In addition, the emission lines at 18 493, 18 538, 18 554, and 18 574 cm^{-1} originate from transitions of upper Stark levels of the $^4S_{3/2}$ state to $^4I_{15/2}(x)$ levels. The relative intensity of emission lines from upper Stark levels decreases by reducing the laser power, indicating heating of the sample by the laser. From these results, we conclude that there is no evidence for a phonon bottleneck in 10 nm $NaYF_4$:Yb^{3+},Er^{3+} NCs. In the discussion below we will discuss possible explanations for the apparent differences between the present results and earlier reports on phonon bottleneck effects in Ln-doped NCs.

Optical Spectroscopy of $NaYF_4$:Eu^{3+}. To obtain more evidence for the role of a phonon bottleneck in Ln^{3+}-doped NCs, $NaYF_4$:Eu^{3+} NCs were investigated. The spacing between Stark levels in $NaYF_4$:Er^{3+} is relatively large (up to ~50 cm^{-1}) while the strongest effects are expected for smaller energy gaps which are fully in the region of the acoustic phonon cutoff. The Stark levels of the $^5D_1$ state of europium in $NaYF_4$ are separated by these small energies, typically ~10 cm^{-1}.[37] For this reason, 10 nm $NaYF_4$:Eu^{3+} NCs are ideal to obtain further insight in the presence of phonon bottleneck effects in Ln-doped NCs.

Figure 5a shows emission spectra of bulk $NaYF_4$:Eu^{3+}(0.3%) recorded in the temperature range between 4.2 and 44 K while exciting into the $^5D_2$ level of Eu^{3+} at 465.2 nm (21 496 cm^{-1}) with a pulsed laser (peak intensity is 42 kW/cm^2). The emission spectrum recorded at 4.2 K shows one emission line at 19 040 cm^{-1}, which is assigned to the $^5D_1$–$^7F_0$ transition. Again, only the lowest Stark level of the excited state is populated at 4.2 K. For this reason, the emission line originates from the $^5D_1(1)$ level to the nondegenerate $^7F_0$ state. The emission spectra recorded at 23 and 44 K show three emission lines at 19 040, 19 050, and 19 072 cm^{-1} (see Figure 5a). At higher temperatures, the upper Stark levels of the excited state are populated. As a result, the three emission lines correspond to transitions from the $^5D_1(x)$ levels to the $^7F_0(1)$ level. The positions of these emission lines agree reasonably well with the 19 013, 19 055, and 19 076 cm^{-1} previously reported in literature.[34,37] The energy gap between the $^5D_1(1)$ level and the $^5D_1(2)$ and $^5D_1(3)$ levels are 10 and 32 cm^{-1}, respectively, which makes this system ideal to investigate the presence of the phonon bottleneck in Ln-doped NCs.

In order to investigate the presence of the phonon bottleneck in $NaYF_4$:Eu^{3+} (0.5%) NCs, emission spectra were recorded at temperatures between 2.2 and 44 K. Figure 5b shows normalized emission spectra of NCs excited at 465.2 nm (21 496 cm^{-1}) with a peak intensity of 42 kW/cm^2. The emission spectra of NCs show three emission peaks positioned at 19 040, 19 050, and 19 072 cm^{-1} at temperatures higher than 4.2 K, originating from transitions of the three $^5D_1(x)$ levels to the $^7F_0(1)$ level. Just as for the bulk sample, the emission lines from transitions of upper Stark levels disappear when lowering the temperature to 4.2 K. As in some of the reports on phonon bottleneck effects in Ln-doped NCs the temperature was lowered even below 4.2 K, we also recorded an emission spectrum of the NCs at 2.2 K (see Figure 5b). A single emission line is observed at 19 040 cm^{-1} which is ascribed to the $^5D_1(1)$–$^7F_0(1)$ transition. No emission from the Stark levels 10 and 32 cm^{-1} higher in energy is observed. This indicates that there is no evidence for a phonon bottleneck in 10 nm $NaYF_4$:Eu^{3+} NCs. To understand why, in spite of phonon confinement, relaxation to the lowest Stark level is faster than emission, possible relaxation mechanisms will be discussed in the next section.

The high-energy side of the $^5D_1(1)$–$^7F_0(1)$ transition shows at 4.2 K a higher emission intensity than at 2.2 K. The emission shoulder of the emission peak at 4.2 K can be assigned to the $^5D_1(2)$–$^7F_0(1)$ transition. Based on the Boltzmann distribution,

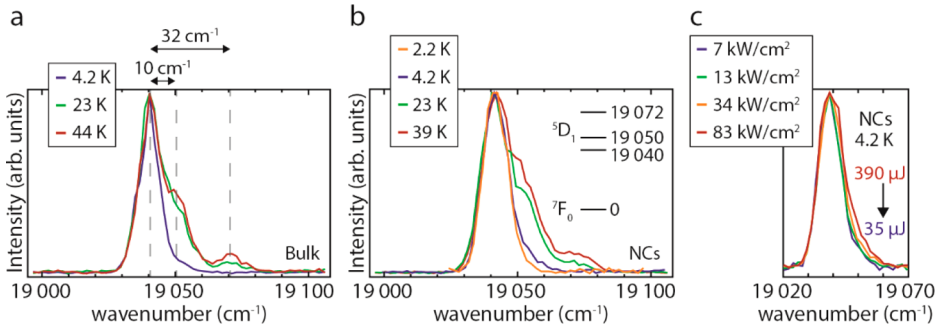

Figure 5. Emission spectra (λ_{exc} = 465.2 nm, pulsed laser) of (a) microcrystalline and (b) nanocrystalline $NaYF_4$:Eu^{3+} showing the $^5D_1$–$^7F_0$ transition recorded at various temperatures measured with a peak intensity of 42 kW/cm^2. Part of the energy level diagram of Eu^{3+} in $NaYF_4$ is shown in (b). (c) Emission spectra of NCs at 4.2 K showing the $^5D_1$–$^7F_0$ transition recorded with excitation powers ranging from 35 to 390 μJ per pulse, corresponding to peak intensities of 7 to 83 kW/cm^2, respectively.

DOI: 10.1021/acs.jpcc.7b11171
J. Phys. Chem. C 2018, 122, 3985–3993

the $^5D_1(2)$ level is populated by 2.7% at 4.2 K. In order to investigate the influence of heating by the excitation source on the luminescence properties of the NCs, emission spectra were recorded with various excitation powers at 4.2 K. Figure 5c shows emission spectra with excitation powers varying from 35 to 390 μJ per pulse (peak intensities of 7 to 83 kW/cm^2). Reducing the excitation power decreases the emission intensity of the emission shoulder, indicating that also here laser-induced heating is responsible for the observation of emission from higher Stark levels. At the lowest excitation powers, no emission from upper Stark levels is observed, in spite of the small 10 cm^{-1} separation between the $^5D_1(1)$ and $^5D_1(2)$ levels for which phonon bottleneck effects could be expected based on phonon confinement in 10 nm nanocrystals.

DISCUSSION

Previous studies have reported the presence of a phonon bottleneck in Ln-doped NCs with sizes similar to the nanocrystals reported here.[7,14,18,19] In these studies a variety of NCs doped with different lanthanide dopants were studied and shown to give emission and excitation lines originating from Stark levels which would be expected not to be thermally populated at the temperature at which spectra were recorded. The cutoff energy of acoustic phonon modes depends on the size of the nanocrystals and to a lesser extent on the composition of the host material (via the mass of and bond strength between the host ions). For this reason, the difference of phonon bottleneck effects reported in previous reports and in the present study cannot be explained by the different nature of the host material. It is interesting to try and understand the origin of the difference between these and our present observations. In the experiments reported by Liu et al.[14,19] the nanocrystalline samples were measured in evacuated quartz cells with 1 Torr of He gas. In this configuration the connection between the nanocrystals and the coldfinger of the cryostat is characterized by a very poor thermal conductivity. Both the low gas pressure (insulating) and the quartz ampule may result in heating of the sample. The particles are in a low pressure insulation environment and not in direct contact with the coldfinger. Poor thermal conductivity through the quartz and vacuum surrounding the NCs may result in laser-induced heating. Further experimental explorations are needed to unravel the mechanism responsible for the hot emission lines in Ln-doped NCs.

The present study was aimed at observing emission from higher Stark levels. For this emission to occur, the phonon relaxation rates have to be strongly reduced from the commonly observed ~ps range to the ~ms range where it can compete with (parity forbidden) radiative decay from the higher Stark levels. Clearly, the factor of 10^9 reduction in relaxation rates is extreme, and even if there is a considerable reduction in phonon relaxation rate due to the absence or low density of resonant phonon states, there still can be no observable emission from higher Stark levels. It cannot be excluded that relaxation is in fact slowed down resulting in longer dephasing times as observed in photon echo experiments, but not sufficiently slow to observe emission from these levels. There is evidence from photon echo experiments that phonon-induced dephasing is slower in nanostructures due to phonon confinement effects. The present study cannot exclude or confirm these effects as only emission spectra and no coherence lifetimes were measured. To probe an influence of phonon confinement on shorter time scales, phonon-induced relaxation processes need to be probed. The coherence time of excited states of lanthanide ions in nanocrystals can be compared with that in bulk material. Specifically, photon echo experiments to measure the temperature-dependent dephasing time of the $^5D_1$ state of Eu^{3+} would be insightful. At low temperatures, direct processes (absorption and emission of phonons resonant with the small energy differences between the $^5D_1$ crystal field components) are expected to dominate the dephasing of the $^5D_1$ excited state, resulting in a longer coherence time for the $^5D_1$ state for Eu^{3+} in nanocrystals if phonon bottleneck effects are present. Some research has been done on the homogeneous linewidth for Ln^{3+} ions in nanocrystals and suggests a larger homogeneous line width (i.e., faster dephasing) in nanocrystals, contrary to what would be expected if phonon bottleneck effects slow down direct phonon relaxation.[7] In a recent report no difference was found in homogeneous linewidth for bulk and nanocrystals. It is clear that further research is required to understand the role of phonon confinement on the optical properties of Ln^{3+}-doped nanocrystals.[38]

The calculations of phonon density of states for ~10 nm nanocrystals predict a phonon cutoff around 10−20 cm^{-1} and sparse, discrete phonon modes at higher energies. It is interesting to try and understand how in the absence of resonant phonon modes relaxation between Stark levels can still take place. It is possible that as the particles are in a condensed form, contact between particles (in spite of the capping ligands) allows more extended lower energy acoustic phonon modes in connected nanoparticles.[39] Also, the phonon modes may not be confined to the nanocrystalline core but extend to the substrate or ligands in contact with the nanocrystals.[39,40] Finally, also two-phonon relaxation processes involving the absorption and emission of higher energy phonons may already occur at cryogenic temperatures despite very low phonon occupation numbers of the higher energy phonons involved. Temperature-dependent measurements of excited state coherence times of lanthanide ions in bulk and nanocrystals can provide insightful information on the relaxation mechanism.

It is expected that phonon bottleneck effects are stronger as the NCs become smaller since the cutoff energy of acoustic phonon modes shifts to higher acoustic phonon energies for smaller sizes. In the present study we investigated monodisperse nanocrystals of sizes similar to those for which phonon bottleneck effects have been previously reported. As we find no confirmation for these effects, it is interesting to investigate the presence of the phonon bottleneck in smaller NCs and in different host materials, e.g., 4 nm YVO_4 NCs. Clearly, further research is required to confirm and quantify the role of the changes in the low energy acoustic phonon spectrum and phonon bottleneck effects at cryogenic temperatures in Ln-doped NCs.

CONCLUSIONS

The role of the phonon bottleneck in relaxation processes for Ln-doped nanocrystals (NCs) was investigated. For this purpose, high resolution emission spectra of micro- and nanocrystalline $NaYF_4$ samples doped with different Ln^{3+} ions (Ln = Er, Yb, Eu) were recorded at cryogenic temperatures with pulsed and continuous wave excitation sources operating at various excitation intensities. Emission from 10 to 55 cm^{-1} upper Stark levels is observed for Er^{3+}- and Eu^{3+}-doped NCs at low temperatures. However, the relative emission intensity of

DOI: 10.1021/acs.jpcc.7b11171
J. Phys. Chem. C 2018, 122, 3985−3993

transitions from upper Stark levels decreases when the excitation power is reduced, and no emission from upper Stark levels is observed at the lowest excitation intensities. This indicates that the NCs are heated by the excitation source, resulting in emission from upper Stark levels. From this, we conclude that phonon bottleneck effects do not affect the emission spectra of 10 nm Ln-doped $NaYF_4$ NCs and that these Ln-doped NCs have the same emission spectra as their microcrystalline analogues at low excitation powers. The absence or reduced density of states of low energy acoustic phonon modes in these NCs does not result in nonthermal equilibrium emission from closely spaced Stark levels as was previously reported. Further research into the role of phonon bottleneck effects in Ln-doped NCs is however interesting. The present study clearly indicates that measurements on phonon bottleneck effects have to be performed carefully to exclude the influence of laser-induced heating.

AUTHOR INFORMATION

Corresponding Author

*E-mail A.Meijerink@uu.nl; Tel +31 30 253 2202 (A.M.).

ORCID

Jacobine J. H. A. van Hest: 0000-0001-9665-6220

Celso de Mello Donega: 0000-0002-4403-3627

Andries Meijerink: 0000-0003-3573-9289

Notes

The authors declare no competing financial interest.

ACKNOWLEDGMENTS

The research leading to these results has received funding from European Union's Seventh Framework Programme FP7/2007-2013/for project GUIDEnano under grant agreement no. 604387.

REFERENCES

(1) Bouzigues, C.; Gacoin, T.; Alexandrou, A. Biological Applications of Rare-Earth Based Nanoparticles. *ACS Nano* **2011**, *5*, 8488−8505.

(2) Dong, H.; Du, S.-R.; Zheng, X.-Y.; Lyu, G.-M.; Sun, L.-D.; Li, L.-D.; Zhang, P.-Z.; Zhang, C.; Yan, C.-H. Lanthanide Nanoparticles: From Design toward Bioimaging and Therapy. *Chem. Rev.* **2015**, *115*, 10725−10815.

(3) Huang, X.; Han, S.; Huang, W.; Liu, X. Enhancing Solar Cell Efficiency: The Search for Luminescent Materials as Spectral Converters. *Chem. Soc. Rev.* **2013**, *42*, 173−201.

(4) Lamb, H. On the Vibrations of an Elastic Sphere. *Proc. London Math. Soc.* **1881**, *13*, 189−212.

(5) Tamura, A. Smoothed Density of States of Electrons and Smoothed Frequency Spectrum of Phonons for a Mesoscopic System. *Phys. Rev. B: Condens. Matter Mater. Phys.* **1995**, *52*, 2668−2677.

(6) Tamura, A.; Higeta, K.; Ichinokawa, T. Lattice Vibrations and Specific Heat of a Small Particle. *J. Phys. C: Solid State Phys.* **1982**, *15*, 4975−4991.

(7) Meltzer, R. S.; Hong, K. S. Electron-Phonon Interactions in Insulating Nanoparticles: Eu_2O_3. *Phys. Rev. B: Condens. Matter Mater. Phys.* **2000**, *61*, 3396−3403.

(8) Inoshita, T.; Sakaki, H. Electron-Phonon Interaction and the so-called Phonon Bottleneck Effect in Semiconductor Quantum Dots. *Phys. B* **1996**, *227*, 373−377.

(9) Bockelmann, U.; Bastard, G. Phonon Scattering and Energy Relaxation in Two-, One-, and Zero-Dimensional Electron Gases. *Phys. Rev. B: Condens. Matter Mater. Phys.* **1990**, *42*, 8947−8951.

(10) Urayama, J.; Norris, T. B.; Singh, J.; Bhattacharya, P. Observation of Phonon Bottleneck in Quantum Dot Electronic Relaxation. *Phys. Rev. Lett.* **2001**, *86*, 4930−4933.

(11) Mukai, K.; Ohtsuka, N.; Shoji, H.; Sugawara, M. Emission from Discrete Levels in Self-Formed InGaAs/GaAs Quantum Dots by Electric Carrier Injection: Influence of Phonon Bottleneck. *Appl. Phys. Lett.* **1996**, *68*, 3013−3015.

(12) Oron, D.; Aharoni, A.; de Mello Donega, C.; van Rijssel, J.; Meijerink, A.; Banin, U. Universal Role of Discrete Acoustic Phonons in the Low-Temperature Optical Emission of Colloidal Quantum Dots. *Phys. Rev. Lett.* **2009**, *102*, 177402.

(13) de Wijn, H. W. Phonon Physics in Ruby Studied by Optical Pumping and Luminescence. *J. Lumin.* **2007**, *125*, 55−59.

(14) Restricted Phonon Relaxation and Anomalous Thermalization of Rare Earth Ions in Nanocrystals Liu, G. K.; Zhuang, H. Z.; Chen, X. Y. *Nano Lett.* **2002**, *2*, 535−539.

(15) Bednarkiewicz, A.; Maczka, M.; Strek, W.; Hanuza, J.; Karbowiak, M. Size Dependence on Infrared Spectra of $NaGdF_4$ Nanocrystals. *Chem. Phys. Lett.* **2006**, *418*, 75−78.

(16) Bünzli, J.-C. G. The Europium(III) Ion as Spectroscopic Probe in Bioinorganic Chemistry. *Inorg. Chim. Acta* **1987**, *139*, 219−222.

(17) Binnemans, K. Interpretation of Europium(III) Spectra. *Coord. Chem. Rev.* **2015**, *295*, 1−45.

(18) Tissue, B. M. Synthesis and Luminescence of Lanthanide Ions in Nanoscale Insulating Hosts. *Chem. Mater.* **1998**, *10*, 2837−2845.

(19) Liu, G. K.; Chen, X. Y.; Zhuang, H. Z.; Li, S.; Niedbala, R. S. Confinement of Electron-Phonon Interaction on Luminescence Dynamics in Nanophosphors of Er^{3+}:Y_2O_2S. *J. Solid State Chem.* **2003**, *171*, 123−132.

(20) Schietinger, S.; Menezes, L. S.; Lauritzen, B.; Benson, O. Observation of Size Dependence in Multicolor Upconversion in Single Yb^{3+}, Er^{3+} Codoped $NaYF_4$ Nanocrystals. *Nano Lett.* **2009**, *9*, 2477−2481.

(21) Wang, J.; Song, H.; Xu, W.; Dong, B.; Xu, S.; Chen, B.; Yu, W.; Zhang, S. Phase Transition, Size Control and Color Tuning of $NaREF_4$:Yb^{3+},Er^{3+} (RE = Y, Lu) Nanocrystals. *Nanoscale* **2013**, *5*, 3412−3420.

(22) Malyukin, Y. V.; Masalov, A. A.; Zhmurin, P. N. Single-Ion Fluorescence Spectroscopy of a Y_2SiO_5:Pr^{3+} Nanocluster. *Phys. Lett. A* **2003**, *316* (1−2), 147−152.

(23) Liu, L.; Ma, E.; Li, R.; Liu, G.; Chen, X. Effects of Phonon Confinement on the Luminescence Dynamics of Eu^{3+} in Gd_2O_3 Nanotubes. *Nanotechnology* **2007**, *18*, 015403.

(24) Yang, H. S.; Hong, K. S.; Feofilov, S. P.; Tissue, B. M.; Meltzer, R. S.; Dennis, W. M. Electron-Phonon Interaction in Rare Earth Doped Nanocrystals. *J. Lumin.* **1999**, *83*−*84*, 139−145.

(25) Mittleman, D. M.; Schoenlein, R. W.; Shiang, J. J.; Colvin, V. L.; Alivisatos, A. P.; Shank, C. V. Quantum Size Dependence of Femtosecond Electronic Dephasing and Vibrational Dynamics in CdSe Nanocrystals. *Phys. Rev. B: Condens. Matter Mater. Phys.* **1994**, *49*, 14435−14447.

(26) Aarts, L.; van der Ende, B. M.; Meijerink, A. Downconversion for Solar Cells in $NaYF_4$:Er,Yb. *J. Appl. Phys.* **2009**, *106*, 023522.

(27) Park, J.; An, K.; Hwang, Y.; Park, J.-G.; Noh, H.-J.; Kim, J.-Y.; Park, J.-H.; Hwang, N.-M.; Hyeon, T. Ultra-Large-Scale Syntheses of Monodisperse Nanocrystals. *Nat. Mater.* **2004**, *3*, 891−895.

(28) Rinkel, T.; Raj, A. N.; Dühnen, S.; Haase, M. Synthesis of 10 nm β-$NaYF_4$:Yb,Er/$NaYF_4$ Core-Shell Upconversion Nanocrystals with 5 nm Particle Cores. *Angew. Chem., Int. Ed.* **2016**, *55*, 1164−1167.

(29) Li, Z.; Zhang, Y. An Efficient and User-Friendly Method for the Synthesis of Hexagonal Phase $NaYF_4$:Yb,Er/Tm Nanocrystals with Controllable Shape and Upconversion Fluorescence. *Nanotechnology* **2008**, *19*, 345606.

(30) Wang, F.; Deng, R.; Liu, X. Preparaton of Core-Shell $NaGdF_4$ Nanoparticles Doped with Luminescent Lanthanide Ions to be Used as Upconversion-Based Probers. *Nat. Protoc.* **2014**, *9*, 1634−1644.

(31) Tong, L.; Lu, E.; Pichaandi, J.; Zhao, G.; Winnik, M. A. Synthesis of Uniform $NaLnF_4$ (Ln Sm to Ho) Nanoparticles for Mass Cytometry. *J. Phys. Chem. C* **2016**, *120*, 6269−6280.

(32) Ellens, A.; Andres, H.; Meijerink, A.; Blasse, G. Spectral-Line-Broadening Study of the Trivalent Lanthanide-Ion Series. I. Line

DOI: 10.1021/acs.jpcc.7b11171
J. Phys. Chem. C 2018, 122, 3985−3993

Broadening as a Probe of the Electron-Phonon Coupling Strength. *Phys. Rev. B: Condens. Matter Mater. Phys.* **1997**, *55*, 173−179.
(33) Renero-Lecuna, C.; Martín-Rodríguez, R.; Valiente, R.; González, J.; Rodríguez, F.; Krämer, K. W.; Güdel, H. U. Origin of the High Upconversion Green Luminescence Efficiency in β-$NaYF_4$:Er^{3+},20%Yb^{3+}. *Chem. Mater.* **2011**, *23*, 3442−3448.
(34) Tu, D.; Liu, Y.; Zhu, H.; Li, R.; Liu, L.; Chen, X. Breakdown of Crystallographic Site Symmetry in Lanthanide-Doped $NaYF_4$ Crystals. *Angew. Chem., Int. Ed.* **2013**, *52*, 1128−1133.
(35) van Hest, J. J. H. A.; Blab, G. A.; Gerritsen, H. C.; de Mello Donega, C.; Meijerink, A. Probing the Influence of Disorder on Lanthanide Luminescence using Eu-doped $LaPO_4$ Nanoparticles. *J. Phys. Chem. C* **2017**, *121*, 19373−19382.
(36) Suyver, J. F.; Grimm, J.; van Veen, M. K.; Biner, D.; Krämer, K. W.; Güdel, H. U. Upconversion Spectroscopy and Properties of $NaYF_4$ Doped with Er^{3+}, Tm^{3+} and/or Yb^{3+}. *J. Lumin.* **2006**, *117*, 1−12.
(37) Zakaria, D.; Fournier, M. T.; Mahiou, R.; Cousseins, J. C. On Eu^{3+} Luminescence in the Hexagonal $NaYF_4$ Phase. *J. Alloys Compd.* **1992**, *188*, 250−254.
(38) Bartholomew, J. G.; de Oliveira Lima, K.; Ferrier, A.; Goldner, P. Optical Line Width Broadening Mechanisms at the 10 kHz Level in Eu^{3+}:Y_2O_3 Nanoparticles. *Nano Lett.* **2017**, *17*, 778−787.
(39) Geller, M. R.; Dennis, W. M.; Markel, V. A.; Patton, K. R.; Simon, D. T.; Yang, H.-S. Theory of Electron-Phonon Dynamics in Insulating Nanoparticles. *Phys. B* **2002**, *316-317*, 430−433.
(40) Yang, Y.-S.; Geller, M. R.; Dennis, W. M. Noninertial Mechanism for Electronic Energy Relaxation in Nanocrystals. *Phys. Rev. B: Condens. Matter Mater. Phys.* **2000**, *62*, 9398−9401.

DOI: 10.1021/acs.jpcc.7b11171
J. Phys. Chem. C 2018, 122, 3985−3993